Review Article

Terahertz and X-Ray Imaging for Ballistic Armor and Related Composites: A Systematic Review of Defect and Post-Impact Assessment

Veri Trisnawan*, Bayu Azmi, and Fery Hadi Setiawan
Research Center for Radiation Process Technology, Research Organization for Nuclear Energy, National Research and Innovation Agency, Tangerang Selatan, Indonesia

Hakimul Wafda
Research Center for Nuclear Reactor Technology, Research Organization for Nuclear Energy, National Research and Innovation Agency, Tangerang Selatan, Indonesia

Adi Abimanyu
Electromechanics Program, Polytechnic Institutes of Nuclear Technology, Sleman, Indonesia
National Research Tomsk Polytechnic University, Tomsk, Russia

Maykel Manawan
Faculty of Defense Technology, Indonesia Defense University, Bogor, Indonesia

*Corresponding author. E-mail: veri.trisnawan@brin.go.id DOI: 10.14416/j.asep.2026.11.013
Received: 7 September 2026; Revised: 8 October 2026; Accepted: 2 November 2026; Published online: 26 November 2026
© 2026 King Mongkut's University of Technology North Bangkok. All Rights Reserved

Abstract
Ballistic composite armor contains aramid/Kevlar, polymer, ceramic, adhesive, and hybrid layers where internal damage may be visually hidden. This Scopus-based systematic review assesses terahertz (THz) and X-ray imaging for defect detection, depth interpretation, and post-impact characterization in ballistic armor and related composites. The final search retrieved 308 records; 51 journal articles from 2020-2026 met the eligibility criteria. Five studies directly addressed ballistic, body-armor, or military-designated systems, whereas 46 offered transferable evidence from adjacent composites. In selected nonmetallic armor configurations, THz identified cracks, delamination, missing material, shrinkage, and subsurface anomalies. X-ray radiography enables projection imaging; X-ray computed tomography (XCT) and micro-computed tomography (micro-CT) reconstruct internal damage volumes when specimen dimensions and laboratory access permit. Evidence supports configuration-dependent complementarity, not universal modality rankings. Defect depth, imaging metadata, uncertainty, external validation, and links to residual ballistic resistance are reported inconsistently. We propose conditional modality selection based on material architecture, defect morphology and provenance, depth, access, resolution needs, and inspection objective. Priorities include probability-of-detection qualification, head-to-head testing on identical realistic armor, external validation of artificial-intelligence models, and links between imaging indications, residual ballistic performance, and acceptance criteria.

Keywords: Ballistic composite armor, Delamination, Nondestructive evaluation, Post-impact assessment, Terahertz imaging, X-ray computed tomography

1 Introduction

Ballistic protection relies on deliberately heterogeneous armor systems in which aramid/Kevlar fabrics, polymer matrices, ceramic strike faces, adhesives, and hybrid interfaces jointly dissipate projectile energy. Their safety function depends not only on constituent strength but also on interface integrity, reinforcement continuity, manufacturing quality, and post-impact condition. Inspection is therefore part of the armor safety case rather than an ancillary quality-control step, because visual examination alone cannot establish whether hidden defects have compromised protective performance

[1]. Figure 1 summarizes the layered architecture and defect locations that motivate the review.

The inspection challenge is intensified by composite damage mechanics. Localized impact can generate matrix cracking, fiber fracture, interfacial debonding, ply splitting, delamination, crushing, and permanent through-thickness deformation even when surface evidence is limited. Adjacent impact studies show that barely visible damage may reduce compression-after-impact strength and that XCT can reveal delamination growth, ply splitting, and morphology-dependent residual behavior [2]–[8], [9]. These studies are not substitutes for ballistic evidence, but they show why armor disposition requires depth-resolved internal assessment rather than surface screening alone.

Terahertz (THz) and X-ray imaging exploit complementary physical contrasts. X-ray radiography provides attenuation-based two-dimensional projections, whereas X-ray computed tomography (XCT) reconstructs volumes; micro-computed tomography (micro-CT) offers finer voxels over a smaller field of view. Non-ionizing THz interrogates dielectric interfaces in aramid, glass-fiber-reinforced polymer (GFRP), quartz-fiber-reinforced polymer (QFRP), and related nonmetallic stacks, with time-domain echoes supporting depth interpretation [10]–[15]. Carbon-fiber-reinforced polymer (CFRP) attenuates THz through conductive, orientation-dependent fiber networks.

Direct THz investigations detected cracks, delamination, material absence, shrinkage, and inserted subsurface flaws in selected aramid/military composites; some features were clearer than in comparator X-ray projections under the reported conditions [16], [17]. Reflection-mode terahertz time-domain spectroscopy (THz-TDS) also resolved layer-related responses in alumina/Kevlar/polyurethane armor with projectile-hit damage and localized moisture [18].

Direct XCT work on ballistic aramid-reinforced panels combined mesoscale architecture with post-impact delamination and deformation [19]. Body-armor evaluation also identifies radiography and ultrasonics within a wider reliability-assessment portfolio [1]. This evidence supports XCT for laboratory volumetric characterization when specimen size and access allow, not universal full-panel field inspection.

Armor-specific evidence is embedded in a wider composite-NDE literature spanning aerospace and structural systems. Adjacent studies inform imaging, depth localization, automation, and validation, but differences in layer architecture, moisture, curvature, strike faces, loading rates, and acceptance criteria restrict direct transfer to armor.

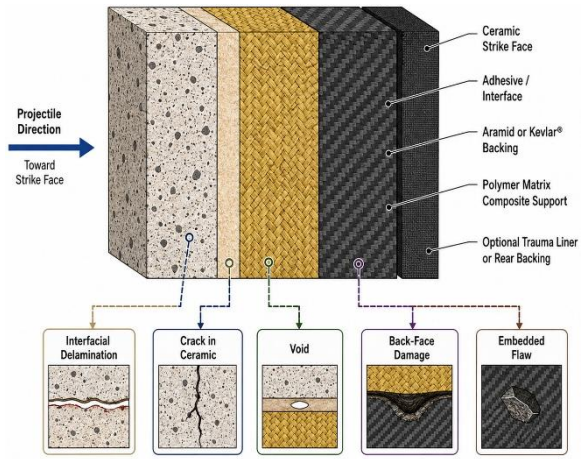


Figure 1: Representative multilayer architecture of ballistic and military-designated composite armor as well as typical locations of internal flaws.

This review separates direct armor evidence from transferable composite evidence and examines studied materials, manufacturing/service/impact defects, modality-specific contrast and depth/resolution, quantitative validation, and barriers to deployment. Its evidence hierarchy distinguishes five direct armor studies from adjacent investigations rather than pooling modality rankings. We argue for decision-driven selection based on material architecture, defect morphology and provenance, target depth/resolution, inspection access, and the consequences of false acceptance or rejection.

2 Methods

2.1 *Review design and reporting*

This systematic review synthesizes empirical THz, radiography, XCT/micro-CT, and relevant comparator evidence in ballistic, military-designated, protective, and materially adjacent composites. Reporting addresses applicable PRISMA 2020 items: identification, screening, eligibility, inclusion, information sources, search, selection, extraction, synthesis, and limitations [20]. Heterogeneous materials, damage generation, acquisition, outcomes, and validation precluded statistical pooling; descriptive counts, evidence tables, and critical narrative synthesis kept direct and adjacent evidence separate.

2.2 *Information source and search strategy*

The review was designed a priori as a Scopus-based systematic review. The final search was executed on 2 September 2026 using the TITLE-ABS-KEY field. Scopus was selected as the sole bibliographic source because its broad engineering/materials coverage and fielded Boolean syntax supported a reproducible, consistently filtered corpus. Web of Science and IEEE Xplore were not searched because the protocol defined a single-database corpus rather than a post hoc multi-database expansion; Google Scholar was not used as the primary systematic source because ranked retrieval and coverage are less reproducible for a fixed review query. This choice improves within-database reproducibility but may omit records indexed only elsewhere and is treated as a review limitation.

Exact Scopus search string: TITLE-ABS-KEY(("nondestructive evaluation" OR "non-destructive testing" OR NDE OR NDT) AND (radiation OR radiography OR "X-ray" OR tomography OR "computed tomography" OR CT OR neutron OR gamma OR terahertz OR "digital radiography") AND ("ballistic composite*" OR "composite armor" OR "armor material*" OR "protective composite*" OR "fiber reinforced polymer" OR FRP OR Kevlar OR aramid OR UHMWPE) AND (damage OR defect* OR delamination OR crack* OR porosity OR inspection OR characterization))

2.3 *Eligibility criteria*

Eligible publications were English-language journal articles dated 2020 to 2 September 2026 on imaging-based THz, X-ray/digital radiography, XCT/micro-CT, phase/dark-field contrast, digital tomosynthesis, or explicit THz-X-ray fusion. Comparator NDE was included only when relevant to validation or cross-modality interpretation. Direct evidence concerned ballistic armor, body armor, bullet-resistant equipment, or military-designated composites; adjacent evidence covered relevant aramid/Kevlar, GFRP, CFRP, QFRP, hybrid-fiber, and ceramic/polymer systems. The prespecified 2020 cutoff prioritized contemporary digital THz, CT reconstruction, and AI-assisted imaging; omitted pre-2020 foundational evidence is acknowledged as a limitation and may be cited only contextually. Pre-2020, non-article, non-English, unrelated, mechanical-only without imaging linkage, and otherwise out-of-scope records were excluded.

2.4 *Screening and study selection*

Of 308 Scopus records, sequential exclusion removed 137 pre-2020 papers, 54 non-articles, five non-English reports, and 61 outside the material/method/damage scope, leaving 51 (308 - 137 - 54 - 5 - 61 = 51). Titles/abstracts were screened against eligibility criteria; full texts were consulted where relevance remained uncertain. No report was unavailable. Available records do not document duplicate independent screening or adjudication, so these procedures are not claimed; their absence is a review limitation. Distinct publications by Pałka *et al.* [18], [21] and by Strąg and Świderski [16], [17] were retained as separate study records. Figure 2 presents the identification, screening, eligibility, and inclusion flow.

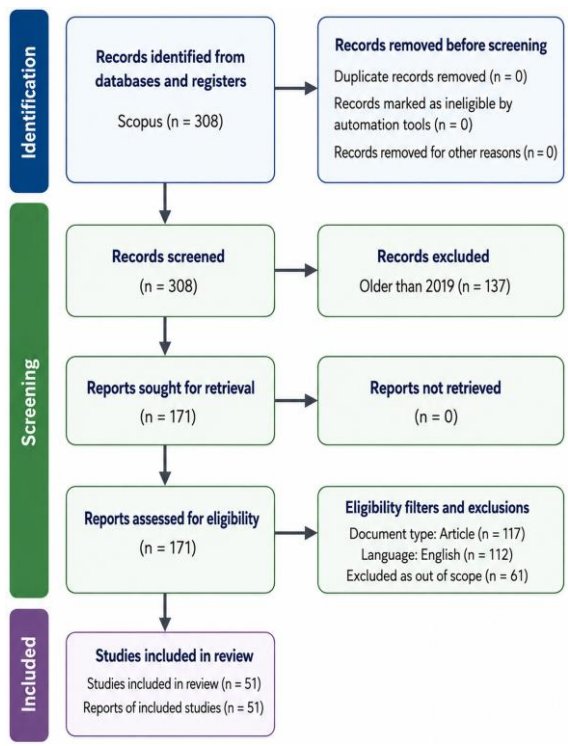


Figure 2: PRISMA flow diagram summarizing identification, screening, eligibility assessment, and final inclusion of studies.

2.5 *Data extraction and classification*

Extraction recorded material/architecture, application context, imaging modality and acquisition, defect provenance/class, depth-resolution route, quantitative outcome, validation/ground truth, principal findings, and evidence role. Provenance was categorized as artificial/inserted, manufacturing-generated, service/environmental, low-velocity/quasi-static impact, or ballistic/projectile-generated where reported. Absolute dimensional, relative/percentage, localization/depth, segmentation/classification errors, and measurement uncertainty were kept distinct. AI studies were also assessed for dataset size, class balance, data split, accuracy, sensitivity/recall, specificity, precision, F1/AUC where applicable, and external validation. Coding yielded 22 THz-led, 28 X-ray/CT-led, and one dedicated THz-X-ray fusion study, stratified by direct or adjacent evidence. Table 1 summarizes the comparative evidence and modality-specific constraints. Supplementary Tables S1 and S2 document study-level coding and AI reporting, respectively.

2.6 *Synthesis and appraisal approach*

Six synthesis domains were evaluated: direct ballistic evidence, material effects, detectability, depth/three-dimensional measurement, post-impact relevance, and validation/automation/deployment. Because designs and outcomes were heterogeneous, a common

Table 1: Comparative evidence matrix for THz and X-ray imaging in ballistic armor and related composite NDE.

Modality / Strategy	Best Supported Use Case	Defect Classes	Depth / Quantification Route	Main Strength and Limitation
THz transmission imaging	Aramid/polymer military composites; noncontact, non-ionizing inspection	Cracks, delamination, lack of material, shrinkage, embedded flaws at depth	Time-domain/through-thickness depth contrast; area scans	Direct aramid feasibility depends on specimen, scanner, and sufficient transmission.
THz-TDS reflection imaging	One-sided multilayer ceramic/Kevlar/polyurethane armor inspection	Interfaces, hidden damage, projectile hits, moisture-affected zones	Time-of-flight, B-scans/C-scans, cross-sections, transfer-matrix modelling	Direct feasibility; requires stack-specific transfer-matrix modelling and calibration.
X-ray radiography / digital radiography	Projection-based quality checks of ballistic/protective composites	Internal flaws, voids, drill damage, impact-related discontinuities	2D projection contrast; digital detector arrays; image processing	2D depth overlap and radiation controls; contrast depends on specimen/setup.
X-ray computed tomography / micro-CT	Laboratory reference and post-impact 3D reconstruction	Delamination, deformation, internal geometry, porosity, cracks, projectile damage	3D reconstruction, segmentation, volume rendering, meso-/macro-scale scans	Direct/adjacent 3D evidence; limits include field of view, voxel size, time, handling, cost, shielding, field access.
X-ray digital tomosynthesis / phase contrast	Planar/limited-angle inspection when XCT is impractical	Ply wrinkles, matrix cracking, subtle contrast features	Limited-angle depth inference; phase/dark-field/attenuation contrast	Advanced X-ray contrast; direct ballistic evidence remains sparse.
THz + X-ray fusion	GFRP/FRP multi-depth defects; contrast/resolution trade-offs	Delamination and inclusions	Image fusion, saliency/wavelet transforms, weighted optimization	One adjacent GFRP study supports conditional complementarity; no direct ballistic fusion evidence.
AI-assisted THz/X-ray interpretation	Automated classification or quantification in complex/high-volume inspection	Delamination, debonding, pores, cracks, impact damage	CNNs, Transformers, U-Net++, lightweight networks, feature fusion	Adjacent metrics vary by data and validation; armor-specific external tests remain needed.
Multimodal validation strategy	Armor-NDE ground truth / validation	All target defect classes	XCT/micro-CT or destructive/mechanical comparators for THz/radiography	Ground truth must match the claimed quantity; no universal protocol.

numerical risk-of-bias score was inappropriate. Evidential confidence was instead assessed by armor directness, damage/loading realism, independent ground truth, and availability of quantitative findings.

The same appraisal fields were applied to each study and coded as reported, partially reported, not reported, or not applicable. Fields covered material architecture; defect class, size, depth, orientation, and provenance; imaging settings and spatial/voxel resolution; geometry, calibration, and reconstruction; validation; metric type/uncertainty; external testing; and links to residual mechanical/ballistic response. Table 2 summarizes the reporting-quality appraisal domains, observed limitations, and minimum expectations for future studies; study-level traceability is provided in Supplementary Table S1.

3 Theoretical Background

3.1 *Ballistic and military-designated composite armor systems*

Ballistic armor is an engineered stack: aramid/Kevlar provides tensile energy absorption, polymers transfer load, ceramic strike faces disrupt projectiles, and bonds/coatings maintain layer continuity. Examples include body-armor components, alumina/Kevlar/polyurethane armor, and aramid-fabric-reinforced ballistic panels [1], [17]–[19]. Their interfaces generate useful contrast but also overlapping reflections, scattering, partial-volume effects, and orientation-dependent interference.

THz inspectability depends on dielectric properties and interfacial impedance. Discontinuities in complex permittivity/conductivity at ceramic-polymer or ceramic-metal interfaces generate reflections; conductive metallic layers may screen deeper inspection. Carbon-hybrid networks are lossy and anisotropic, with attenuation and

Table 2: Reporting-quality and comparability appraisal profile of the reviewed evidence base.

Appraisal criterion	Observed pattern in the reviewed evidence	Why it matters for armor NDE	Minimum expectation for future studies
Directness to armor	Five direct ballistic/military studies; remaining evidence is adjacent.	Transfer of performance claims to armor remains conditional.	Separate direct/adjacent evidence and state transfer limits.
Defect description	Defect type often reported; size, depth, orientation, and location not standardized.	Modality comparison depends on comparable target defects.	Report defect class, dimensions, depth, orientation, and generation method.
Defect provenance	Inserted, manufacturing, service, low-velocity/quasi-static, and projectile damage are distinct.	Detectability from controlled inserts may not transfer to naturally generated ballistic damage.	Report provenance/loading history; assess transfer separately.
Imaging metadata	Frequency/bandwidth, X-ray settings, resolution, geometry, reconstruction, and calibration inconsistently specified.	Apparent superiority may reflect acquisition settings rather than modality capability.	Provide modality settings, reconstruction, and calibration.
Quantification and uncertainty	Visibility, classification, dimensional, localization, segmentation, and uncertainty metrics differ.	Armor disposition requires traceable confidence in size and depth estimates.	Specify metric type, ground truth, absolute/relative errors, uncertainty, and PoD if qualifying.
Validation route	Ground truth ranged from comparator NDE and XCT to destructive, mechanical, and simulation methods.	Ground truth should match the target quantity being claimed.	Define the reference standard for presence, size, depth, morphology, and structural relevance.
AI/deployment readiness	AI datasets, class balance, splits, metrics, and external tests vary or remain unreported.	High test accuracy does not equal readiness for safety-critical decisions.	Report dataset/classes, splits, accuracy, recall, specificity, precision, F1/AUC, confidence, external tests, failures.
Residual performance link	Few studies link imaging indications to residual resistance or acceptance thresholds.	Inspection value ultimately depends on disposition decisions.	Couple imaging metrics with residual mechanical or ballistic performance and decision criteria.

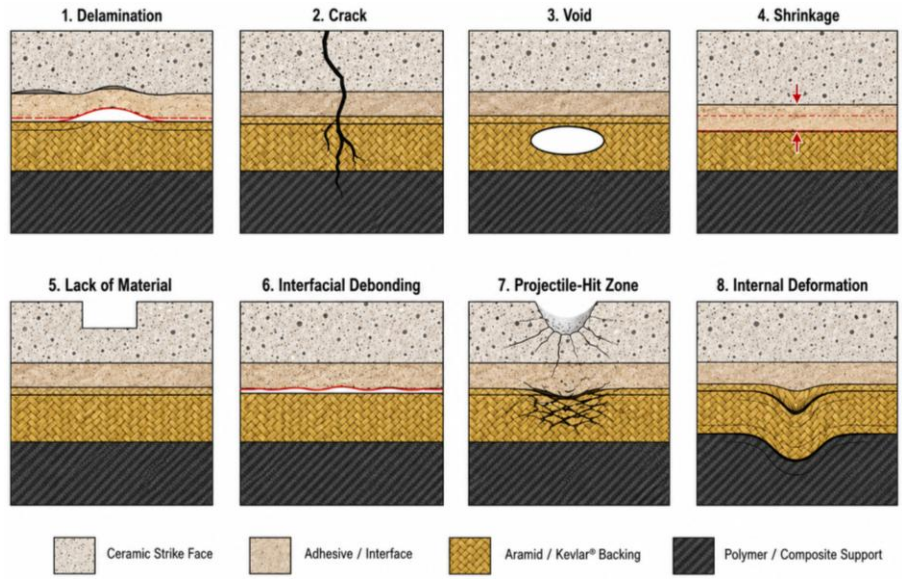


Figure 3: Schematic illustration of common defects and damage modes in ballistic composite armor.

polarization/orientation effects. Closely spaced ceramic, adhesive, coating, and backing interfaces create multiple or overlapping echoes. Ceramic-hybrid evidence [22] reinforces the structural significance of reinforcement/matrix heterogeneity; signal calibration must represent the actual armor stack rather than a homogeneous approximation.

3.2 *Damage and defect typology*

Manufacturing flaws include porosity, inclusions, missing material, resin-rich/dry zones, fiber misalignment, waviness, drilling damage, incomplete bonding, and foreign layers. Service/impact damage includes matrix cracks, fiber failure, debonding, delamination, ply splitting, crushing, fatigue, back-face deformation, and fragmentation. Direct armor studies reported cracks, delamination, material loss, shrinkage, projectile-hit regions, and panel deformation [16], [18], [19]. Artificial inserts, manufacturing defects, low-velocity impact, and ballistic/projectile damage have different morphologies and loading histories and must remain separate provenance classes.

The inspection result becomes most useful when it specifies not only defect presence but also class, size, depth, volume, orientation, and structural relevance. Adjacent XCT studies show that three-dimensional damage geometry can evolve under subsequent loading and that projected area alone may poorly represent residual behavior [2]–[4], [9]. Figure 3 therefore frames the defect taxonomy used throughout the synthesis.

3.3 *Principles and outputs of terahertz imaging*

THz waves interact with nonconductive composites through reflection, transmission, absorption, phase, and time delay. Continuous-wave imaging maps amplitude/phase; terahertz time-domain spectroscopy (THz-TDS) records pulses for time-of-flight and spectral analysis. A-, B-, and C-scans depict local waveforms, cross sections, and spatial maps. Reflection permits one-sided access; transmission requires both sides and sufficient through-thickness signal [14], [15], [18].

THz performance depends on architecture, thickness, frequency/bandwidth, polarization, scan geometry, signal-to-noise ratio, moisture, curvature, coatings, bonds, ceramic/backing layers, and interfaces. Aramid, Kevlar, GFRP, QFRP, and polymers can offer favorable dielectric contrast, unlike conductive carbon-rich systems. Wavelet denoising, sparse deconvolution, time-window fusion, Fourier/principal-component analysis, CNNs, and Transformers can assist localization, but require calibration, representative training, reference stratigraphy, and external validation [23], [14], [21], [24]–[26].

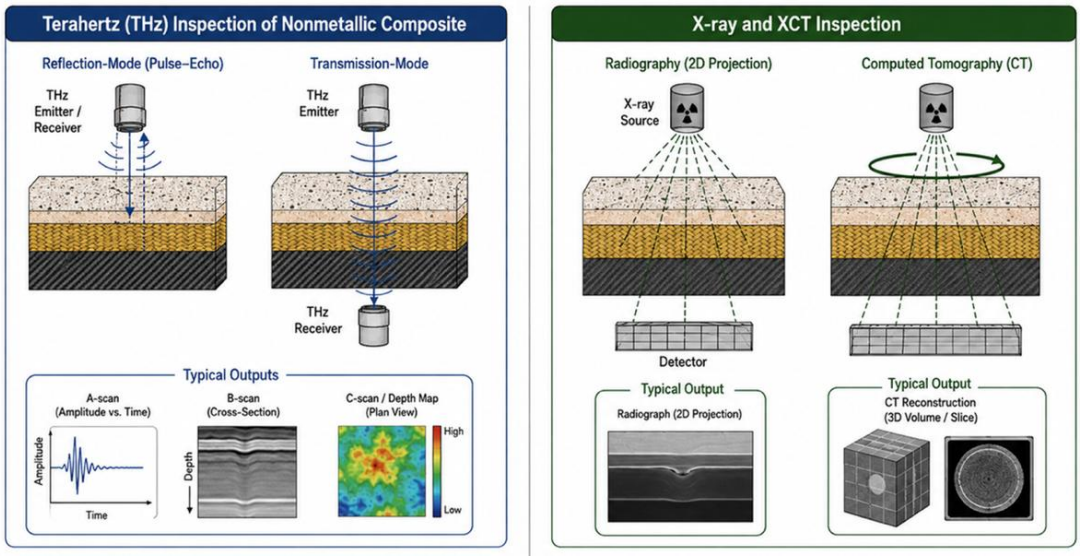


Figure 4: Conceptual comparison of terahertz and X-ray/XCT inspection principles for nondestructive evaluation of ballistic composites.

CFRP and carbon-containing armor require specific caution: conductive fiber networks attenuate THz, alter polarization according to fiber orientation, and obscure deeper interface echoes. Metallic layers can block deeper interrogation; moisture increases absorption and changes dielectric contrast. Curvature changes incidence angle, while coatings/adhesives create reflections that may mimic flaws without layer-by-layer calibration. No universal THz penetration depth applies: frequency band, stack, thickness, moisture, acquisition geometry, and depth-resolution conditions must be reported.

3.4 *Principles and outputs of X-ray radiography and computed tomography*

Here, X-ray imaging is an umbrella term. X-ray radiography denotes attenuation-based 2D projections; X-ray computed tomography (XCT) reconstructs 3D volumes from multiple projections; micro-computed tomography (micro-CT) uses finer voxels, generally within a smaller field of view. Radiography superimposes depths, whereas XCT/micro-CT quantifies pores, crack density, delamination geometry, reinforcement arrangement, and impact deformation. Automated micro-CT also enables pore segmentation and matrix-crack measurements [10], [11], [27], [28].

Phase contrast and Talbot-Lau differential-phase/dark-field methods enhance selected subtle boundaries, transverse cracks, and porosity; digital tomosynthesis offers limited-angle depth information [29]–[31]. X-ray inspections require radiation control and may face artifacts, reconstruction time, and voxel-size/field-of-view trade-offs. XCT is consequently most defensible for laboratory reference, development, forensic, or selected sample assessment rather than unrestricted field scanning. Figure 4 illustrates the distinct THz reflection/transmission, radiographic projection, and XCT acquisition and output routes.

3.5 *Complementarity and decision-support logic*

THz and X-ray encode complementary contrasts. In Wang *et al.,* [32], selected GFRP delamination/inclusion specimens and acquisition settings yielded higher THz defect contrast and finer XCT spatial resolution; fusion improved specified image metrics. This is not a universal ranking or demonstration of ballistic-armor fusion. Method choice must follow material/damage type, required depth and resolution, accessible geometry, validation route, and disposition risk.

No universal THz-'shallower'/X-ray-'deeper' comparison is defensible. THz penetration depends on frequency, dielectric loss, conductivity, thickness, moisture, layer count, and geometry; X-ray transmission depends on spectrum, density, atomic number, thickness,

and projections. Radiography superimposes depth, XCT reconstructs volumes, and THz resolves interfaces only when echoes and refractive calibration permit. Comparative claims require explicit acquisition and material conditions.

4 Review of Findings

4.1 *Study selection and evidence profile*

The PRISMA process in Figure 2 reduced 308 Scopus records from the final search on 2 September 2026 to 51 included publications. The corpus is strongly recent: two studies appeared in 2020, three in 2021, six in 2022, eight in 2023, 14 in 2024, nine in 2025, and nine in 2026. This pattern shows rapid growth in advanced THz processing and quantitative X-ray/CT methods. It should not, however, be interpreted as an equally large armor-specific evidence base because most publications are materially adjacent composite studies.

Only five publications were direct ballistic, defense, or military-designated evidence: body-armor evaluation [1], two aramid THz studies [16], [17], THz-TDS of alumina/Kevlar/polyurethane armor [18], and multiscale XCT of aramid-reinforced polymer ballistic panels [19]. The other 46 publications were adjacent evidence involving relevant materials, defects, impact processes, validation routes, or imaging technologies. Across the 51-study corpus, 22 were coded as THz-led, 28 as X-ray/CT-led, and one as dedicated THz-X-ray fusion (Figure 5). These counts and the direct/adjacent classification are mapped study-by-study in Supplementary Table S1.

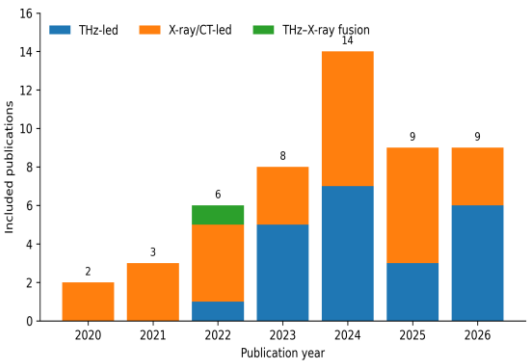


Figure 5: Temporal distribution of included publications by primary modality category.

4.2 *THz imaging of aramid and military-designated composites*

In direct armor evidence, Strąg and Świderski [16] used 100 and 300 GHz THz to detect cracks, delamination, material absence, shrinkage, and features not apparent in comparator X-ray projections. The 300 GHz setting gave finer detail for the tested specimens. These findings are frequency- and configuration-specific, not evidence of universal THz superiority.

A second aramid study [17] detected intentionally embedded plates at different subsurface positions using transmission-mode THz imaging. The result supports controlled quality inspection of sufficiently transmissive aramid laminates when contactless, non-ionizing operation is prioritized. Its transfer to complete armor assemblies depends on thickness, curvature, coverings, moisture, backing materials, and two-sided access.

4.3 *Reflection-mode THz-TDS in ceramic/Kevlar armor*

Pałka *et al.,* [18] directly investigated reflection-mode THz-TDS on alumina strike plates bonded to Kevlar/polyurethane armor. Raster scans of projectile-hit regions, rear mechanical damage, and water-covered zones produced time traces, surface maps, and cross sections for layer-sensitive interpretation. Transfer-matrix modelling aided thickness/defect estimates; multiple reflections and moisture-dependent dielectric changes required stack-specific calibration. The study demonstrates configuration-specific feasibility, not a field performance threshold.

4.4 *X-ray imaging and XCT in ballistic assessment*

Ziółkowski *et al.,* [19] used mesoscale XCT for representative-volume modelling of aramid-fabric polymer ballistic panels and macroscale XCT to quantify delamination and deformation following 38 Special and 9 x 19 mm impacts. The method links architecture, post-impact geometry, and modelling, subject to laboratory specimen-size and access limits.

Body-armor evaluation [1] places radiography and ultrasonics alongside visual inspection and ballistic testing. The direct evidence therefore supports provisional roles: THz for selected dielectric-layer defects, radiography for projection checks, and

XCT for volumetric laboratory or forensic characterization. Figure 6 contrasts practical one-sided, two-sided, and X-ray access configurations rather than demonstrating comparative field performance.

4.5 *THz evidence from materially adjacent composites*

Adjacent THz studies demonstrate depth-related measurement in controlled composites: wavelet-processed THz-TDS improved GFRP delamination thickness estimates [14]; deconvolved time-of-flight tomography resolved laminate thickness and delamination edges [15]; and adaptive window fusion mapped multiple GFRP defect depths, with average relative defect-size errors below 7% in [23]. This percentage measures relative size estimation, not generic classification accuracy or measurement uncertainty. Artificial/embedded flaws mainly establish controlled detectability, not equivalence to naturally generated ballistic damage. Figure 7 illustrates depth-sensitive interpretation.

Fast THz reflection, compressed single-pixel and high-speed imaging, robotics, CNNs, Transformers, and feature-fusion networks have improved selected acquisition and defect-analysis tasks in GFRP, QFRP, Kevlar, and hybrids [21], [24]–[26], [33]–[37], [38]. Additional adjacent studies examined THz monitoring of woven-GFRP deformation [39], bending-related damage in GFRP [40], tensile-induced subsurface damage [41], and THz-based analysis of hygrothermal ageing in composites [42]. Metrics cannot be pooled across different tasks, defect provenance, labels, dataset splits, or validation. Supplementary Table S2 separates AI metric types and reporting completeness.

4.6 *X-ray, radiography, and CT evidence from adjacent composites*

Adjacent XCT/micro-XCT has quantified porosity, constituent fractions, crack density, fracture geometry, and local deformation in CFRP/GFRP and hybrid laminates [10], [11], [27], [28], [43]. Synchrotron micro-CT combined with digital volume correlation [9] linked UD-CFRP microdefects to kink-band development and localized failure mechanics. These measurements inform model calibration but do not directly establish ballistic performance.

Advanced X-ray contrast, limited-angle methods, and projection imaging broaden the design space. Dark-field and differential-phase approaches improve porosity or subtle crack sensitivity, digital tomosynthesis supports ply-wrinkle assessment when

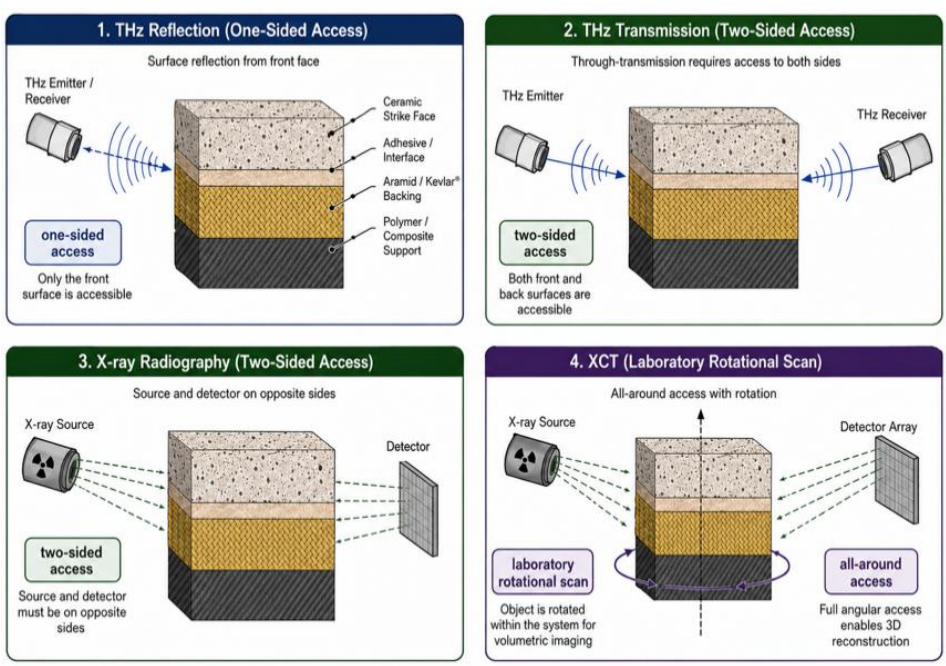


Figure 6: Schematic comparison of inspection configurations.

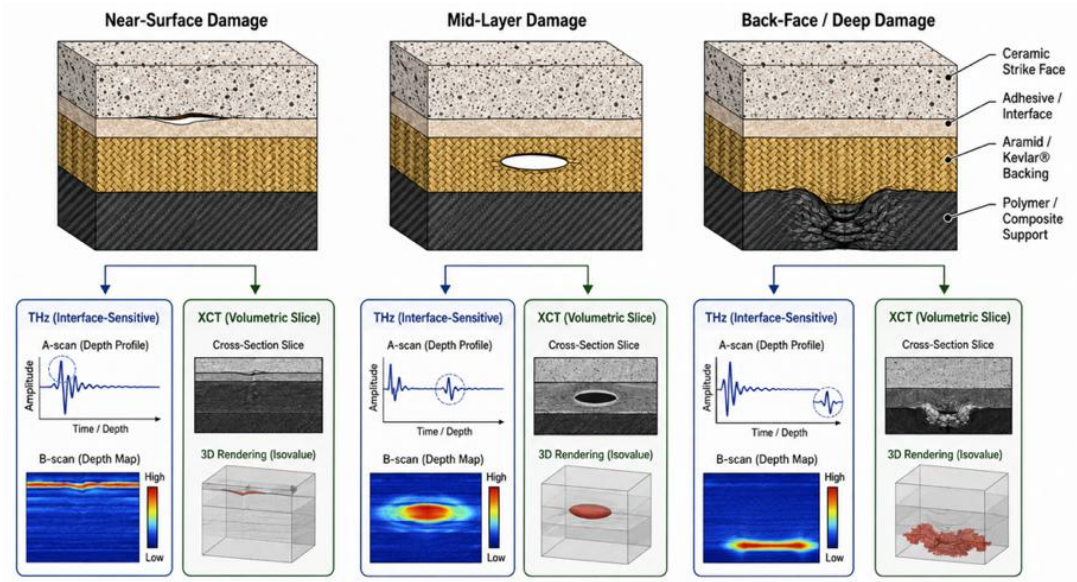


Figure 7: Conceptual illustration of depth-resolved damage interpretation in multilayer armor.

full CT is impractical, and radiography remains relevant to lower-complexity quality inspection and automated image interpretation [29]–[31], [44]–[47]. These applications are not ballistic armor, but they reinforce defect-specific modality selection and scalable manufacturing inspection.

4.7 *Post-impact damage and structural relevance*

Adjacent post-impact XCT studies associate delamination, ply splitting, fiber fracture, debris wedges, environmental states, preload, and laminate design with damage evolution and residual mechanical behavior [2]–[8], [48], [49], [50]. Outside the 51-study THz/X-ray corpus, Mahesh *et al.,* [51] used ultrasonic C-scan after 20-50 J low-velocity impacts on sisal/epoxy: damage area/cracks increased, perforation occurred at 50 J, and maximum deformation approached 22 mm. This contextual result links energy to flaw mapping but cannot be equated with ballistic projectile damage.

4.8 *Validation, fusion, and comparative performance*

Validation used comparator NDE, destructive observation, mechanical testing, and modelling. Ultrasonics/CT quantified selected delamination or drilled defects [12], [13]; synchrotron micro-CT and digital volume correlation resolved local deformation [9]; micro-CT also provided THz ground truth for additively manufactured CFRP [52]. The reference standard must correspond to the claimed property: defect presence, size, depth, morphology, or structural consequence.

The sole dedicated THz-X-ray fusion study [32] assessed GFRP delamination/inclusions: THz provided dielectric contrast, XCT supplied spatial detail, and saliency/wavelet-weighted fusion improved selected image metrics. As an adjacent-composite study, it does not establish ballistic fusion effectiveness. X-ray-ultrasonic fusion [53] and broader modality comparisons [54] suggest complementarity, but require registration, appropriate ground truth, and configuration-specific validation.

4.9 *Reporting-quality appraisal*

Application of the appraisal criteria defined in Section 2.6 revealed inconsistent reporting of defect depth/provenance, acquisition and spatial-resolution metadata, explicit error/uncertainty type, independent validation, and links to residual ballistic performance. Table 2 consolidates these decision-relevant reporting gaps and their recommended reporting requirements, while Supplementary Table S1 provides study-level coding.

4.10 *AI-assisted interpretation and quantitative reporting*

AI performance is reported by task/material rather than pooled. Kim *et al.,* [24] reported 95% classification accuracy for GFRP microdefects below 20 micrometers; Liu *et al.,*. [35] reported class-wise precision of 1.0, 1.0, 1.0, 0.985, and 1.0 and F1 = 0.982 for five inserted QFRP delamination classes; Yan *et al.,* [26] reported 98.40% accuracy on GFRP and 98.63% on QFRP. Silitonga *et al.,* [38] used co-located micro-CT as ground truth for depth-resolved THz analysis of impact-damaged thermoplastics. Class definitions, datasets, splitting, and validation differ, precluding direct rankings; see Supplementary Table S2.

5 Discussion

5.1 *Complementarity rather than substitution*

Direct evidence supports conditional THz inspection of selected dielectric armor layers and XCT characterization of laboratory-compatible post-impact panels [16], [18], [19]. The 46 adjacent studies provide mechanistic context, not 46 additional ballistic experiments. Figure 8 synthesizes complementary screening, characterization, and validation roles without claiming a universal ranking.

5.2 *Material architecture governs inspectability*

Armor architecture governs inspectability. Aramid/Kevlar and analogous GFRP/QFRP can provide THz-sensitive dielectric interfaces; conductive CFRP and hybrids attenuate THz and introduce orientation-dependent polarization effects [52]. Ceramic faces, dense/metal inserts, coatings, adhesives, backing layers, curvature, and moisture further affect echoes and access. Interface heterogeneity also matters mechanically [22]. Accordingly, candidate inspections and calibration should address individual layers/interfaces, not assume a homogeneous armor panel.

5.3 *Defect morphology governs modality performance*

Defect geometry determines contrast and method suitability. Planar delamination can yield THz echoes; pores, complex crack fronts, projectile channels, and volumetric damage can motivate XCT/micro-CT, while transverse cracks may benefit from phase-sensitive X-ray methods. Inserted flaws do not fully

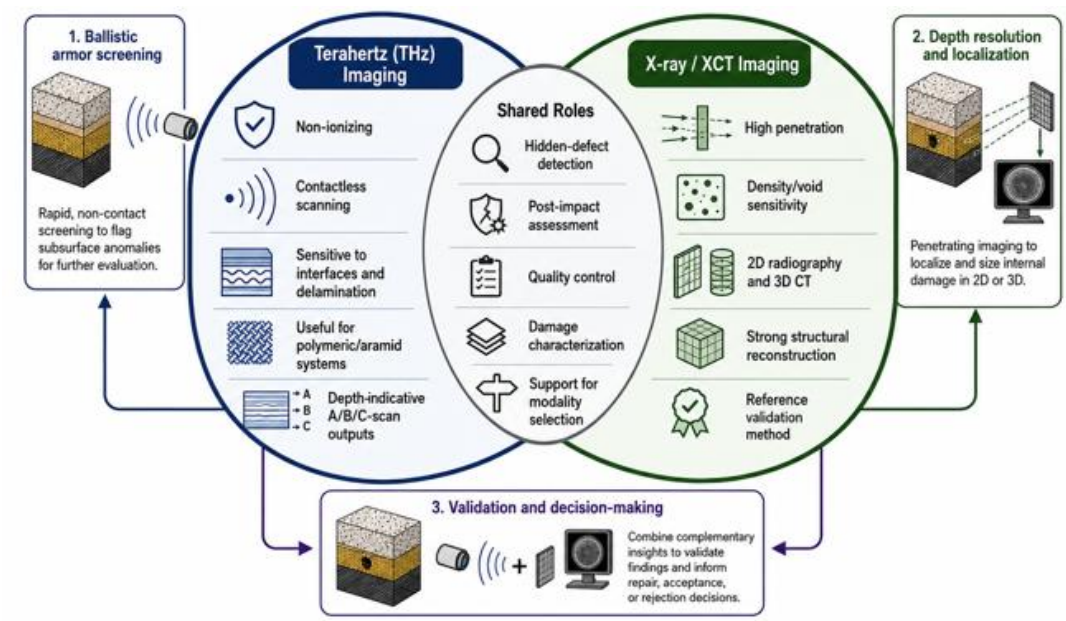


Figure 8: Complementary strengths and shared functions of terahertz and X-ray/XCT imaging in ballistic composite nondestructive evaluation.

represent manufacturing or ballistic damage in roughness, closure, branching, orientation, or strain fields. Inspection specifications must define defect type/provenance, critical size, depth, access, and probability of detection [29], [31], [32].

5.4 *Depth resolution is the decisive performance dimension*

Depth matters because similar projected delamination areas may lie at a strike face, bondline, backing layer, or wearer-side interface. THz depth resolution depends on bandwidth, refractive index, echo separability, thickness, and calibration; XCT resolution depends on voxel size, projection sampling, reconstruction, artifacts, and segmentation. Neither has a universal armor penetration depth. Qualification requires quantified size/depth errors and uncertainty, not visibility alone [23], [14], [15], [28].

5.5 *From laboratory imaging to deployable inspection*

Deployment requires distinct stages: screening for repeatable indications (e.g., suitable THz reflection or radiography), calibrated characterization of flaw position, depth, and extent (THz-TDS or selected limited-angle X-ray methods), and reference validation or forensic reconstruction using XCT/micro-CT where 3D confidence is necessary. Suitability remains material-, geometry-, and access-dependent.

Qualification must progress from image demonstrations to probability-of-detection (PoD) evidence. ASTM E2862-23 specifies hit/miss PoD analysis for measurable discontinuity sizes and binary inspection responses [55]. Armor-relevant qualification should vary target size/depth, layer architecture, environmental condition, operator/scanner, and access; analyze hits/misses with confidence bounds and relate qualified detectable size to a disposition threshold. PoD alone does not establish ballistic acceptability without linkage to residual mechanical/ballistic performance.

Full-panel XCT is constrained by specimen fit and the field-of-view/voxel trade-off. Large/curved armor may need repositioning, multiple scans, or stitching; acquisition/reconstruction time, radiation shielding, controlled areas, equipment footprint, handling, and cost restrict field use, especially for micro-CT. XCT should thus be treated as a laboratory reference, development, sampled-inspection, or forensic tool when 3D detail justifies these constraints.

5.6 *Automation and data fusion*

Automation can accelerate defect interpretation, but controlled-set classification scores do not establish armor readiness. As detailed in Section 4.10 and Supplementary Table S2, published AI metrics refer to differing materials, class distributions, label definitions, tasks, and train/test strategies; they are not directly comparable. Impact-damage THz classification with co-located micro-CT ground truth [38] strengthens validation. Deployment still requires independent tests across armor batches, scanners, geometries, moisture conditions, and realistic flaw populations.

Contextual non-imaging ML studies [56], [57] illustrate task-specific reporting: thermoplastic-nanocomposite property prediction used regression metrics (R-squared, RMSE, MAE, MSE), while tribological prediction reported R-squared. These studies are outside the 51-study imaging corpus. Supplementary Table S2 instead tracks classification, segmentation, regression, validation splits, and external tests for imaging AI; the blanket term 'accuracy' is inadequate.

Fusion evidence also remains provisional: the sole dedicated GFRP THz-X-ray study [32] did not evaluate ballistic armor. Registration errors, calibration mismatch, and modality-specific uncertainty must be quantified before fused images could support acceptance or rejection decisions.

5.7 *Evidence gaps and review limitations*

Only five studies directly evaluated ballistic/military armor; most quantitative advances derive from adjacent composites with inserted defects or low-velocity/quasi-static loading. Projectile impact differs in strain rate, fragmentation, pressure fields, and coupled damage, preventing direct equivalence. Further limitations include a single Scopus source, omission of pre-2020 studies, undocumented independent screening/adjudication, incomplete defect/acquisition metadata and PoD/uncertainty, scarce residual-ballistic correlations, and few identical-specimen THz-XCT comparisons.

5.8 *Proposed modality-selection framework*

Our six-variable modality-selection framework evaluates material architecture, defect morphology/provenance, target depth, inspection access, required spatial/depth resolution, and inspection objective. It identifies conditional candidates, not a

universally 'preferred' technology: THz reflection for accessible dielectric interfaces; transmission THz for transmissive stacks with two-sided access; radiography for 2D projection checks; limited-angle tomosynthesis for selected depth questions; and XCT/micro-CT for scanner-compatible laboratory 3D characterization. Each option requires attention to evidence directness, acquisition constraints, and validation.

For each armor layer, the inspector specifies flaw class, critical dimensions, provenance, location/depth, and screening versus quantitative or reference objectives before evaluating access and resolution. AI is part of this calibrated measurement chain, not an independent ground truth. Table 3 converts these criteria into representative conditional choices and explicitly labels their evidence constraints.

5.9 *Qualification, standards, and acceptance criteria*

Inspection acceptance is distinct from ballistic qualification. NIJ Standard 0101.07 defines torso-body-armor ballistic requirements and test methods [58] but not THz/XCT defect-acceptance thresholds. A detectable NDE indication therefore cannot independently justify acceptance or rejection. Qualification should demonstrate measurement capability and PoD [55], link measured flaw geometry/location to residual mechanical or ballistic performance, define uncertainty-aware disposition limits, and validate them across representative armor, curvature, environments, and damage states. Standards and contextual sources [22], [51], [55]–[58] inform qualification, impact mapping, interface behavior, and modelling rather than adding to the 51 empirical imaging studies. Figure 9 summarizes the validation pathway from initial imaging indications through independent reference measurements and quantitative interpretation to a confidence-informed inspection decision.

Table 3: Decision matrix for candidate imaging modalities in ballistic armor and related composites.

Material / architecture. Defect, depth, and provenance	Access / objective / resolution need	Candidate modality and evidence constraint
Aramid/polymer-rich layers. Planar delamination, missing material, shrinkage; near-surface to resolvable internal interfaces; artificial or service/impact damage	One-sided screening; non-ionizing; moderate-to-high depth discrimination where echoes separate	THz reflection / THz-TDS. Direct aramid/armor feasibility exists [16], [18], but performance is stack-, frequency-, moisture-, and geometry-dependent.
Transmissive aramid or dielectric laminate. Embedded inclusion/delamination through thickness; controlled defects most common	Two-sided access; screening/localization	THz transmission. Direct military-designated aramid evidence exists [17]; applicability decreases with attenuation, thickness, coverings, or inaccessible back face.
Ceramic/Kevlar/polymer stack. Interfacial damage, projectile-hit region, moisture-related contrast; layered depth interpretation	One-sided characterization; layer-sensitive output	Reflection THz-TDS as a candidate [18]; requires stack-specific dielectric/transfer-matrix calibration and control of multiple reflections.
Large or curved armor panel. Density discontinuity, void, crack or gross damage where exact depth is not essential	Rapid projection-based quality check; practical access to X-ray source/detector	Digital radiography. Provides 2D projection; depth superposition and radiation controls limit direct localization.
Coupon, subcomponent, or scanner-compatible armor. Complex cracks, pores, delamination volume, projectile channel, deformation	Laboratory reference/validation; high 3D geometric confidence	XCT/micro-CT. Direct ballistic-panel evidence exists [19], but field of view, voxel size, scan time, cost, shielding, and panel handling constrain deployment.
Multimodal case with complementary contrast. Defect not sufficiently characterized by a single modality	Reference study or method development with robust registration	THz + X-ray fusion only as experimental candidate. One adjacent GFRP study [33]; no direct ballistic fusion evidence identified.

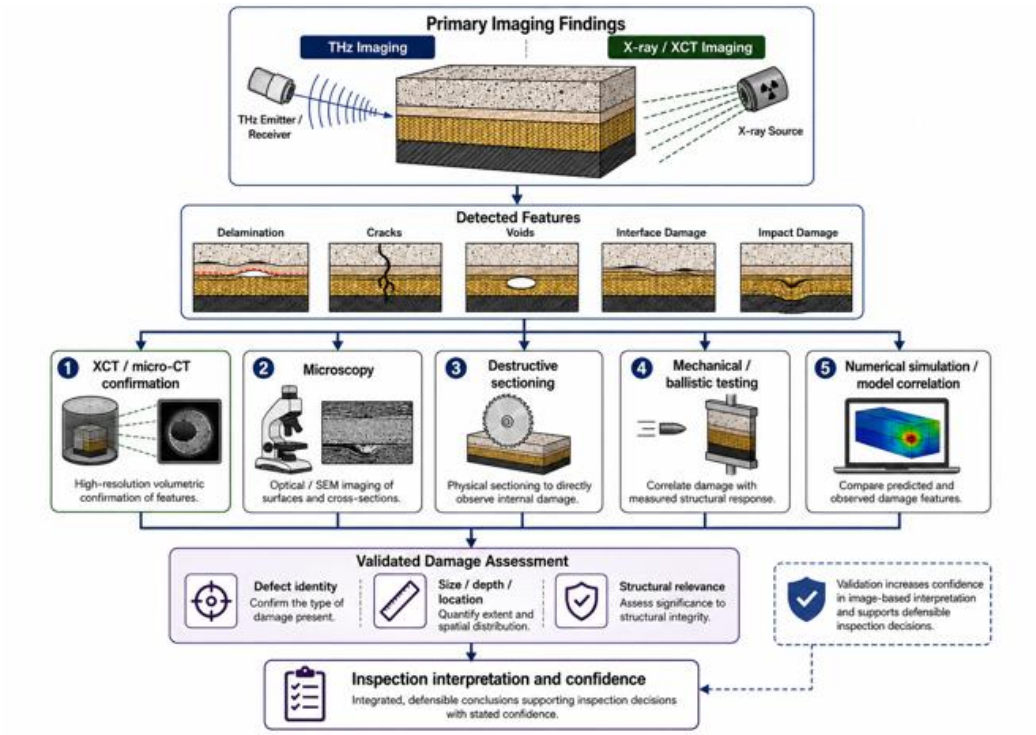


Figure 9: Validation pathway for imaging-based defect and damage assessment.

6 Conclusion

This Scopus-based review synthesized 51 THz/X-ray imaging studies in armor and related composites: five directly examined ballistic/body-armor or military-designated systems, and 46 provided adjacent methodological evidence. Armor-specific conclusions must therefore remain conditional.

Direct studies demonstrate THz sensitivity to selected aramid and ceramic/Kevlar defects and layer responses under reported configurations; radiography supports projection inspection, and XCT resolves post-impact 3D geometry in laboratory-compatible ballistic panels. Adjacent studies inform depth measurement, volumetric analysis, AI, and multimodal fusion but do not establish ballistic equivalence. One GFRP THz-X-ray fusion study cannot establish fusion performance in armor.

Future work should standardize defect provenance, depth, acquisition/resolution settings, metric definitions, uncertainty, and PoD; compare modalities on identical realistically damaged armor; validate imaging AI across scanners and batches; quantify fusion-registration uncertainty; and link NDE indications to residual ballistic resistance and justified acceptance criteria. These are research/qualification priorities, not established field-deployment capabilities.

Author Contributions

V.T.: conceptualization, investigation, reviewing and editing, funding acquisition, project administration.; B.A., H.W., and A.A.: investigation, methodology, writing an original draft; F.H.S.: research design, data analysis; M.M.: conceptualization, data curation, writing—reviewing and editing. All authors have read and agreed to the published version of the manuscript.

Conflicts of Interest

The authors declare no conflict of interest.

Declaration of generative AI and AI-assisted technologies in the writing process

The authors utilized the ChatGPT tool to enhance the language and readability of the manuscript.

Appendix A. Supplementary data

Supplementary data to this article can be found online here.

References

[1] S. Das, N. P. Gunaseelan, and V. Mathivanan, "Ballistic evaluation of body armour for defence application," *Materials Protection*, vol. 66, no. 4, pp. 764–775, Dec. 2025, doi: 10.62638/ZasMat1210.

[2] N. Li, J. Du, H. M. Lee, W. Liu, Y. Zheng, and H. P. Lee, "Damage characterization and modelling of FRP laminated composites subjected to external edge-on impact," *Composites Part B: Engineering*, vol. 287, Dec. 2024, Art. no. 111879, doi: 10.1016/j.compositesb.2024.111879.

[3] V. S. Anuse, S. K., R. Velmurugan, S. K. Ha, and H. Han, "Effect of graphene nano-platelets on the low-velocity-impact and compression-after-impact strength of the glass fiber epoxy composite laminates," *Journal of Composite Materials*, vol. 58, no. 5, pp. 601–618, Mar. 2024, doi: 10.1177/00219983241228833.

[4] V. S. Anuse, K. Shankar, R. Velmurugan, and S. K. Ha, "Compression-after-impact analysis of carbon fiber reinforced composite laminate with different ply orientation sequences," *International Journal of Impact Engineering*, vol. 167, Sep. 2022, Art. no. 104277, doi: 10.1016/j.ijimpeng.2022.104277.

[5] P. Arkuszyński and M. Rośkowicz, "Influence of preloading on damage in CFRP composite material subjected to low-energy impact loads," *Materials*, vol. 18, no. 17, Sep. 2025, Art. no. 4016, doi: 10.3390/ma18174016.

[6] A. Banik, C. Zhang, D. Panyathong, and K. T. Tan, "Effect of equienergetic low-velocity impact on CFRP with surface ice in low temperature arctic conditions," *Composites Part B: Engineering*, vol. 236, May 2022, Art. no. 109850, doi: 10.1016/j.compositesb.2022.109850.

[7] L. Gerdes, S. Richle, S. Mrzljak, D. Hülsbusch, G. Barandun, and F. Walther, "Computed tomography-based characterization of impact and fatigue after impact behavior of carbon fiber-reinforced polyurethane," *Composite Structures*, vol. 289, Jun. 2022, Art. no. 115474, doi: 10.1016/j.compstruct.2022.115474.

[8] M. A. A. Mohsin, L. Iannucci, and E. S. Greenhalgh, "Experimental and numerical analysis of low-velocity impact of carbon fibre-based non-crimp fabric reinforced thermoplastic composites," *Polymers*, vol. 13, no. 21, Nov. 2021, Art. no. 3642, doi: 10.3390/polym13213642.

[9] J. Srisuriyachot et al., "Synchrotron micro-CT in kink-band formation of UD-CFRP laminates with microdefects," *Composites Part B: Engineering*, vol. 266, Nov. 2023, Art. no. 111038, doi: 10.1016/j.compositesb.2023.111038.

[10] E. Dilonardo, M. Nacucchi, F. De Pascalis, M. Zarrelli, and C. Giannini, "High resolution X-ray computed tomography: A versatile non-destructive tool to characterize CFRP-based aircraft composite elements," *Composites Science and Technology*, vol. 192, May 2020, Art. no. 108093, doi: 10.1016/j.compscitech.2020.108093.

[11] E. Dilonardo, M. Nacucchi, F. De Pascalis, M. Zarrelli, and C. Giannini, "Inspection of carbon fibre reinforced polymers: 3D identification and quantification of components by X-ray CT," *Applied Composite Materials*, vol. 29, no. 2, pp. 497–513, Apr. 2022, doi: 10.1007/s10443-021-09976-x.

[12] D. A. Jack, P. Kokkada Ravindranath, K. Matalgah, and T. Fleck, "Quantification of drill hole damages in CFRP laminates using high-resolution ultrasonic testing," *IEEE Open Journal of Instrumentation and Measurement*, vol. 3, pp. 1-9, Oct. 2024, Art. no. 4500409, doi: 10.1109/OJIM.2024.3487238.

[13] K. Matalgah, P. K. Ravindranath, D. Pulipati, and T. J. Fleck, "Automated quantification of interlaminar delaminations in carbon-fiber-reinforced polymers via high-resolution ultrasonic testing," *Polymers*, vol. 15, no. 24, Dec. 2023, Art. no. 4691, doi: 10.3390/polym15244691.

[14] W. Nsengiyumva, S. Zhong, M. Luo, and B. Wang, "Terahertz spectroscopic characterization and thickness evaluation of internal delamination defects in GFRP composites," *Chinese Journal of Mechanical Engineering*, vol. 36, no. 1, Jan. 2023, Art. no. 6, doi: 10.1186/s10033-022-00829-7.

[15] M. Zhai, A. Locquet, and D. S. Citrin, "Terahertz nondestructive layer thickness measurement and delamination characterization of GFRP laminates," *NDT and E International*, vol. 146, Sep. 2024, Art. no. 103170, doi: 10.1016/j.ndteint.2024.103170.

[16] M. Strąg and W. Swiderski, "Defect detection in aramid fiber-reinforced composites via terahertz radiation," *Journal of Nondestructive Evaluation,* vol. 42, no. 1, Mar. 2023, Art. no. 9, doi: 10.1007/s10921-022-00917-7.

[17] M. Strąg and W. Świderski, "Non-destructive inspection of military-designated composite

materials with the use of terahertz imaging," *Composite Structures*, vol. 306, Feb. 2023, Art. no. 116588, doi: 10.1016/j.compstruct.2022.116588.

[18] N. Pałka, K. Kamiński, M. Maciejewski, D. Pacek, and W. Świderski, "Terahertz nondestructive testing of alumina-based ceramic ballistic protection armor," *Infrared Physics and Technology*, vol. 137, Mar. 2024, Art. no. 105163, doi: 10.1016/j.infrared.2024.105163.

[19] G. Ziółkowski, J. Pach, D. Pyka, T. Kurzynowski, and K. Jamroziak, "X-ray computed tomography for the development of ballistic composite," *Materials*, vol. 13, no. 23, pp. 1–19, Dec. 2020, doi: 10.3390/ma13235566.

[20] M. J. Page et al., "The PRISMA 2020 statement: An updated guideline for reporting systematic reviews," *BMJ*, vol. 372, Mar. 2021, Art. no. n71, doi: 10.1136/bmj.n71.

[21] N. Pałka, K. Kamiński, M. Maciejewski, K. Dragan, and P. Synaszko, "Automatic histogram-based defect detection in glass fibre reinforced polymer composites using terahertz time-domain spectroscopy reflection imaging," *Optics and Lasers in Engineering*, vol. 174, Mar. 2024, Art. no. 107959, doi: 10.1016/j.optlaseng.2023.107959.

[22] S. B. Nagaraju, M. Puttegowda, M. K. Somashekara, T. G. Thyavihalli Girijappa, P. D. Govindaswamy, and K. Sathyanarayana, "Advancing the performance of ceramic-reinforced aluminum hybrid composites: A comprehensive review and future perspectives," *Applied Science and Engineering Progress*, vol. 17, no. 2, Apr.–Jun. 2024, Art. no. 7034, doi: 10.14416/j.asep.2023.10.001.

[23] R. Li et al., "Adaptive fusion imaging for delamination defects in GFRP composites based on terahertz time-domain spectroscopy," *Optics and Laser Technology*, vol. 197, May 2026, Art. no. 114863, doi: 10.1016/j.optlastec.2026.114863.

[24] H.-S. Kim, D.-W. Park, S.-I. Kim, G.-H. Oh, and H.-S. Kim, "Non-destructive detection of thin micro-defects in glass reinforced polymer composites using a terahertz electro–magnetic wave based on a convolution neural network," *Composites Part B: Engineering*, vol. 257, May 2023, Art. no. 110694, doi: 10.1016/j.compositesb.2023.110694.

[25] Y. Xu et al., "Full scale promoted convolution neural network for intelligent terahertz 3D characterization of GFRP delamination," *Composites Part B: Engineering*, vol. 242, Aug. 2022, Art. no. 110022, doi: 10.1016/j.compositesb.2022.110022.

[26] S. Yan et al., "A three-branch time-frequency feature fusion method based on terahertz signals for identifying delamination defects in composite materials," *Sensors*, vol. 26, no. 8, Apr. 2026, Art. no. 2429, doi: 10.3390/s26082429.

[27] M. Salgado, J. M. Guerrero, L. Carreras, and J. Renart, "An automated image processing method to detect progressive matrix cracking in CFRP composites using X-ray micro-computed tomography," *Journal of Nondestructive Evaluation*, vol. 45, no. 3, Sep. 2026, Art. no. 104, doi: 10.1007/s10921-026-01387-x.

[28] M. Wang, B. Zhang, S. Zhan, L. Yang, L. Jiang, and Y. Wang, "Micro-computed tomography non-destructive testing and defect quantitative analysis of carbon fiber-reinforced polymer, glass fiber-reinforced polymer and carbon/glass hybrid laminates using deep learning recognition," *Applied Sciences*, vol. 15, no. 22, Nov. 2025, Art. no. 12192, doi: 10.3390/app152212192.

[29] J. Glinz, B. Plank, J. Gutekunst, M. Scheerer, S. Zabler, J. Kastner, and S. Senck, "A comparison of X-ray attenuation, differential phase, and dark-field contrast imaging for the detection of porosity in carbon fiber reinforced cyanate ester," *NDT and E International*, vol. 147, Oct. 2024, Art. no. 103194, doi: 10.1016/j.ndteint.2024.103194.

[30] R. C. V. V. Gomes et al., "Assessment of out-of-plane ply waviness in carbon-fibre reinforced plastics: Comparing different non-destructive evaluation modalities," *NDT and E International*, vol. 160, Jun. 2026, Art. no. 103630, doi: 10.1016/j.ndteint.2026.103630.

[31] O. Helps et al., "Assessment of planar NDE methods for damage in open hole carbon fibre laminates," *NDT and E International*, vol. 154, Sep. 2025, Art. no. 103393, doi: 10.1016/j.ndteint.2025.103393.

[32] J. Wang et al., "Nondestructive damage evaluation of composites based on terahertz and X-ray image fusion," *NDT and E International*, vol. 127, Apr. 2022, Art. no. 102616, doi: 10.1016/j.ndteint.2022.102616.

[33] P. Fosodeder et al., "Fast terahertz reflection imaging for in-line detection of delaminations in glass fiber-reinforced polymers," *Sensors*, vol. 25, no. 3, Feb. 2025, Art. no. 851, doi: 10.3390/s25030851.

[34] A. M. Latha, K. Kabilan, S. Esampelly, and S. Bertleja, "Nondestructive testing of GFRP composites with compressive sensing-based terahertz single-pixel imaging," *Nondestructive Testing and Evaluation*, vol. 40, no. 12, pp.

6225–6242, Dec. 2025, doi: 10.1080/10589759.2025.2457575.

[35] Q. Liu, Q. Wang, J. Guo, W. Liu, R. Xia, J. Yu, and X. Wang, "A Transformer-based neural network for automatic delamination characterization of quartz fiber-reinforced polymer curved structure using improved THz-TDS," *Composite Structures*, vol. 343, Sep. 2024, Art. no. 118272, doi: 10.1016/j.compstruct.2024.118272.

[36] X. Wang et al., "Terahertz characterization of internal debonding defects of composites under class imbalance condition using lightweight network," *Mechanical Systems and Signal Processing*, vol. 248, Mar. 2026, Art. no. 114018, doi: 10.1016/j.ymssp.2026.114018.

[37] B. Lamdjad, "High-resolution defect detection in composite materials using terahertz NDT and deep reconstruction," *Proceedings of the Institution of Civil Engineers: Forensic Engineering*, vol. 179, no. 3, pp. 101–115, Sep. 2026, doi: 10.1680/jfoen.25.00031.

[38] D. J. Silitonga et al., "Automated classification of subsurface impact damage in thermoplastic composites using depth-resolved terahertz imaging and deep learning," *Composites Part B: Engineering*, vol. 309, Jan. 2026, Art. no. 113033, doi: 10.1016/j.compositesb.2025.113033.

[39] P. Pomarede, J. Calvo-De La Rosa, P. Antonik, F. Meraghni, D. S. Citrin, D. Rontani, and A. Locquet, "THz-based monitoring of the deformation of the inner woven structure of glass-fiber reinforced polymers," *IEEE Transactions on Terahertz Science and Technology*, vol. 13, no. 4, pp. 396–404, Jul. 2023, doi: 10.1109/TTHZ.2023.3275278.

[40] P. Lopato, G. Psuj, M. Herbko, and I. Spychalski, "Evaluation of static bending caused damage of glass-fiber composite structure using terahertz inspection," *Open Engineering*, vol. 14, no. 1, Oct. 2024, Art. no. 20240088, doi: 10.1515/eng-2024-0088.

[41] M. Zhai et al., "Monitoring tensile-induced subsurface damages of woven glass fiber reinforced polymer using terahertz time-of-flight tomography," *NDT and E International*, vol. 160, May 2026, Art. no. 103645, doi: 10.1016/j.ndteint.2026.103645.

[42] C. A. Marinho et al., "Machine learning applied to terahertz signal analysis for hygrothermal aging characterization of composites," *Materials* Evaluation, vol. 82, no. 8, pp. 48–58, Aug. 2024, doi: 10.32548/2024.me-04425.

[43] L. Hao, J. Zhang, M. Liu, G. Xu, S. Chen, and X. Li, "Detection of fracture crack in carbon fiber reinforced polymer (CFRP) cables based on microfocus X-ray imaging," *Measurement Science and Technology*, vol. 36, no. 10, Oct. 2025, Art. no. 105403, doi: 10.1088/1361-6501/ae081d.

[44] R. Addanki, P. Mithilesh, and A. Mahajan, "Parametric study on drilling induced damage in thick unidirectional carbon-epoxy composite laminates," *Next Materials*, vol. 13, Oct. 2026, Art. no. 103204, doi: 10.1016/j.nxmate.2026.103204.

[45] N. Bagale and M. R. Bhat, "Evaluation of hygrothermal ageing in CFRP composite material using a non-destructive approach," *Journal of Composite Materials*, vol. 55, no. 10, pp. 1309–1314, May 2021, doi: 10.1177/0021998320967054.

[46] I. Shauqi et al., "Nanoclay effect on the ablative behaviour of glass fiber reinforced polymer and glass fiber reinforced geopolymer nanocomposite using radiography," *Journal of Aeronautics, Astronautics and Aviation*, vol. 56, no. 1, pp. 77–83, 2024, doi: 10.6125/JoAAA.202403_56(1).08.

[47] L. Yang, Y. Wang, D. Miao, and X. Duan, "Damage detection method for high-strength aramid conveyor belts," *IEEE Access*, vol. 13, pp. 2671–2678, 2025, doi: 10.1109/ACCESS.2024.3520204.

[48] T. Dong, Z. Zhao, B. Zheng, C. Chen, and P. Ma, "Response and damage mechanism of carbon/aramid intra-ply hybrid weft-knitted reinforced composites under low-velocity impact," *Thin-Walled Structures*, vol. 196, Mar. 2024, Art. no. 111495, doi: 10.1016/j.tws.2023.111495.

[49] C. Militello, G. Epasto, F. Bongiorno, and B. Zuccarello, "First lamina hybridization of high performance CFRP with Kevlar fibers: Effect on impact behavior and nondestructive evaluation," *Mechanics of Advanced Materials and Structures*, vol. 30, no. 6, pp. 1207–1222, Mar. 2023, doi: 10.1080/15376494.2022.2029639.

[50] J. Wolfrum, S. Eibl, E. Oeltjen, J. Osterholz, and M. Wickert, "High-energy laser effects on carbon fiber reinforced polymer composites with a focus on perforation time," *Journal of Composite Materials*, vol. 55, no. 16, pp. 2249–2262, Jul. 2021, doi: 10.1177/0021998320988885.

[51] S. Mahesh et al., "Influence of incident energy on sisal/epoxy composite subjected to low velocity impact and damage characterization using ultrasonic C-scan," *Applied Science and Engineering Progress*, vol. 15, no. 1, Jan. 2022, Art. no. 5220, doi: 10.14416/j.asep.2021.07.005.

[52] M. Mieloszyk, P. Madejski, S. Wroński, and I. I. Muna, "Structural analyses of additively manufactured carbon fiber reinforced polymer with embedded fiber optic using THz spectroscopy and micro-computed tomography," *Optics and Lasers in Engineering*, vol. 193, Oct. 2025, Art. no. 109086, doi: 10.1016/j.optlaseng.2025.109086.

[53] J. Wang, D. Han, L. Peng, X. Yang, Z. Meng, and J. Zhang, "Non-destructive damage evaluation of composites based on X-ray and ultrasonic image fusion," *Insight: Non-Destructive Testing and Condition Monitoring*, vol. 66, no. 9, pp. 541–547, Sep. 2024, doi: 10.1784/insi.2024.66.9.541.

[54] H. V. Silva, N. P. Catapirra, M. S. Carvalho, T. G. Santos, and M. A. Machado, "Nondestructive testing of 3D printed fiber-reinforced polymeric composites: An experimental critical comparison," *3D Printing and Additive Manufacturing*, vol. 11, no. 3, pp. e1196–e1208, Jun. 2024, doi: 10.1089/3dp.2022.0291.

[55] Standard Practice for Probability of Detection Analysis for Hit/Miss Data, ASTM E2862-23, 2023.

[56] H. Sharma et al., "Predictive modeling of thermoplastic nanocomposites using machine learning algorithms," *Discover Mechanical Engineering*, vol. 4, Nov. 2025, Art. no. 66, doi: 10.1007/s44245-025-00134-2.

[57] D. K. Selvan et al., "Investigation of tribological behaviour of B4C-graphene glass fiber composites using Taguchi, multi-criteria decision making, and machine learning approaches," *Journal of Composite Materials*, Jun. 2026, doi: 10.1177/00219983261450597.

[58] Ballistic Resistance of Body Armor, NIJ Standard 0101.07, 2023.